

# Derivation of nonstationary rainfall intensity-duration-frequency curves considering the impacts of climate change and urbanization

Lei Yan<sup>a,b,\*</sup>, Dongyang Lu<sup>c</sup>, Lihua Xiong<sup>d</sup>, Hongfeng Wang<sup>e</sup>, Qinghua Luan<sup>f</sup>, Cong Jiang<sup>g</sup>, Bin Xiong<sup>h</sup>, Wentao Xu<sup>i</sup>, Pengtao Yan<sup>j</sup>, Qingwen Lei<sup>a,b</sup>, Chong-Yu Xu<sup>k</sup>

<sup>a</sup> College of Water Conservancy and Hydropower, Hebei University of Engineering, Handan 056021, China

<sup>b</sup> Hebei Key Laboratory of Intelligent Water Conservancy, Hebei University of Engineering, Handan 056038, China

<sup>c</sup> Hebei Haochuan Engineering Design Co., Ltd, Shijiazhuang 050000, China

<sup>d</sup> State Key Laboratory of Water Resources and Hydropower Engineering Science, Wuhan Univ., Wuhan 430072, China

<sup>e</sup> Handan Meteorological Bureau of Hebei Province, Handan 056001, China

<sup>f</sup> State Key Laboratory of Hydrology-Water Resources and Hydraulic Engineering, Hohai University, Nanjing 210098, Jiangsu, China

<sup>g</sup> School of Environmental Studies, China University of Geosciences (Wuhan), Wuhan, China

<sup>h</sup> School of Infrastructure Engineering, Nanchang University, Nanchang 330031, China

<sup>i</sup> Changjiang River Scientific Research Institute, Changjiang Water Resources Commission, Wuhan 430010, China

<sup>j</sup> School of Physics and Electronic Engineering, Xingtai University, Xingtai 054001, China

<sup>k</sup> Dept. of Geosciences, Univ. of Oslo, N-0315 Oslo, Norway

## ARTICLE INFO

### Keywords:

Extreme rainfall  
Intensity-duration-frequency curves  
Nonstationary analysis  
Urbanization  
Average annual reliability  
ENSO

## ABSTRACT

Urban infrastructure traditionally relies on stationary rainfall intensity-duration-frequency (IDF) curves. However, this assumption is challenged by climate change and urbanization. Many studies tried to update IDF using time covariate which lacks physical significance. More importantly, the stationary (ST) design method is not applicable for nonstationary (NS) design where the distributions of extreme precipitation change over time. For the annual maximum precipitation (AMP) in Beijing, we utilized local factors (urbanization and temperature) and global factors (ENSO and EASM etc.) to develop NS models, with the average annual reliability method first employed to update the IDF curves. Short-duration (shorter than 6-h) AMP of most stations show upward trends, whereas the AMP with longer durations exhibits downward trends. The NS modeling reveals that the 18-h AMPs is mainly affected by global processes (ENSO and EASM). The predictive accuracy of the optimal NS model outperforms ST model by a remarkable 219% during the validation period. In addition, the ST design rainfall tends to overestimate rainfall for durations longer than 12-h. Interestingly, the gap between NS and ST design uncertainties diminishes as duration/return period expands. The above findings provide new insights about impacts of local and global physical processes on the variation of extreme rainfall.

## 1. Introduction

Rainfall intensity-duration-frequency (IDF) curves are widely used in urban municipal infrastructure design and storm

\* Corresponding author at: College of Water Conservancy and Hydropower, Hebei University of Engineering, Handan 056021, China.

E-mail addresses: [yanl@whu.edu.cn](mailto:yanl@whu.edu.cn) (L. Yan), [xionglh@whu.edu.cn](mailto:xionglh@whu.edu.cn) (L. Xiong), [jiangcong@cug.edu.cn](mailto:jiangcong@cug.edu.cn) (C. Jiang), [xiongb@ncu.edu.cn](mailto:xiongb@ncu.edu.cn) (B. Xiong), [xuwt@mail.crsri.com](mailto:xuwt@mail.crsri.com) (W. Xu), [c.y.xu@geo.uio.no](mailto:c.y.xu@geo.uio.no) (C.-Y. Xu).

management (Endreny and Imbeah, 2009; Bezak et al., 2016; Xu et al., 2018; Kourtis and Tsirhirtzis, 2021). Typically, the rainfall intensities for different durations, ranging from minutes to hours, are calculated by fitting the probability distributions of the annual maximum precipitation series (AMP), and then IDF curves are derived by summarizing the relationships between the precipitation intensity and frequency for different durations (Cheng and Aghakouchak, 2014; Gu et al., 2022). The fundamental assumption of the above theory for deriving IDF curves is that the AMP samples are independent and identically distributed, which is also known as the stationary assumption. In recent decades, however, global temperatures have been rising due to anthropogenic greenhouse gas emissions (Meinshausen et al., 2009; Hansen et al., 2010; Yan et al., 2022a, 2022b; Xu et al., 2023). The increase in temperature allows enhanced atmospheric water storage capacity at a rate of approximately 7%/°C, which in turn leads to an increase in extreme precipitation events (Allen and Ingram, 2002; Feng et al., 2016; Lenderink and Fowler, 2017; Su and Chen, 2019; Zhang et al., 2019). Since the 1950s, either the intensity or the frequency of strong rainfall have increased in most terrestrial regions where observational data are sufficient for trend analysis. Furthermore, as global warming intensifies, strong precipitation events may intensify and become more frequent (IPCC, 2021). Westra et al. (2014) pointed out that the increase in the intensity of sub-daily extreme precipitation events is more significant than that of daily extreme precipitation. In addition, compared with the suburb regions, urban areas are more sensitive to the increasing mainly due to the complicated influence of Urban Heat Island (UHI) on extreme precipitation. It has been reported by many studies that the increase of intensity and/or frequency of urban short-duration extreme precipitation at global scale (Guerreiro et al., 2018; Wu et al., 2019; Fowler et al., 2021; Yue et al., 2022), which is prone to result in more dangerous floods in urban regions (Xiong et al., 2019). On July 20th, 2021, Zhengzhou City, a megacity in North China, suffered an extremely rare heavy precipitation, with the 24-h precipitation reaching 624.1 mm and the maximum hourly precipitation reaching 201.9 mm. The intensity of this disastrous precipitation process broke the historical meteorological record of Chinese mainland, and greatly exceeds the drainage capacity of the urban drainage system. As a result, this disaster killed 380 people and caused losses >40.9 billion CNY. The statistical properties of urban extreme rainfall have been altered by the variation of urban extreme precipitation, and challenged the stationary assumption for municipal engineering design, resulting in the failure of urban infrastructures. Therefore, it is urgent to update the IDF curves to maintain the reliability of municipal projects under a changing environment (Willems, 2013; Cheng and Aghakouchak, 2014; Hassanzadeh et al., 2019; Westra et al., 2014; Mondal and Mujumdar, 2015; Agilan and Umamahesh, 2017; Ganguli and Coulibaly, 2017; Sarhadi and Soulis, 2017; Lima et al., 2018; Wang et al., 2019; Yan et al., 2021b; Kourtis and Tsirhirtzis, 2022).

At present, there are mainly three different ways to update the IDF curves under nonstationary condition, namely the climate-model-based IDF curves (Clim-IDF) and Cov-IDF curves (Cov-IDF) (Yan et al., 2021b; Kourtis and Tsirhirtzis, 2022), and the adaptation method by revising the current IDF curves to account for nonstationarity, ranging from simple constant percentage increase to more complex methods based on Clausius-Clapeyron relationship (Martel et al., 2021). The first method primarily considers future precipitation data downscaled from the climate models as future “observation” data, from which the updated IDF curves are generated. However, several studies have documented that for extreme precipitation, the simulations of climate models have significant biases and uncertainties, resulting in generally low reliability for future projections of extreme precipitation at a given location (Fowler et al., 2007; Alam and Elshorbagy, 2015; Farnham et al., 2018). In recent years, great efforts and advances have been made in developing more powerful climate models with higher resolution to better characterize the physical processes of extreme precipitation, i.e., the regional climate models (RCMs) with 10–50 km spatial resolution and the Convection-permitting models (CPMs) with 4 km spatial resolution (Lenderink and Van Meijgaard, 2008; Evans and Westra, 2012; Zittis et al., 2017). Lucas-Picher et al. (2021) provided a good reference about the improvements of CPMs to model hourly extreme rainfall. However, the power of these advanced physical-based climate models in characterizing the spatial and temporal characteristics of hourly extreme rainfall is unsure, particularly for the long-term precipitation projection in far future (Yan et al., 2021b). Therefore, the Clim-IDF method requires further refinement and development. The second method turns to construct the nonstationary distribution with time-varying statistical parameters to describe the changing properties of AMP based on prescribed covariates (physical covariates or time) for different durations, and estimate the nonstationary design rainfall intensities for various return periods based on the predicted future distributions (Zhu et al., 2016; Ouarda et al., 2019; Vu and Mishra, 2019; Lu et al., 2020; Yan et al., 2021b; Silva et al., 2021; Vinnarasi and Dhanya, 2022). Many studies have tried to update the IDF curves using the Cov-IDF based on the nonstationary Generalized Extreme Value (GEV) distribution with just time covariate. However, this kind of nonstationary distribution lacks physical meaning and may not be the optimal model. Thus, it is important to explore more possible covariates and candidate distributions to better capture the changing characteristics of extreme precipitation (Yuan et al., 2018). Yan et al. (2021a) and Schlef et al. (2023) comprehensively compared and reviewed the difference between Clim-IDF and Cov-IDF and pointed out that research efforts should be paid to reduce the associated uncertainties for both methods and combine the advantages of both methods, besides there is a need for future research on rainfall durations and in regions with seasonal snowmelt.

To compare the performance of the Clim-IDF and Cov-IDF methods in updating IDF curves, Agilan and Umamahesh (2016) not only derived the IDF curves using the downscaled simulations from 24 GCMs, but also updated the IDF curves using the selected best nonstationary distributions with urbanization and El Niño Southern Oscillation (ENSO) covariates. Then, the design rainfall for different return periods yielded using two types of IDF curves are compared, and they found that the design values obtained from the Cov-IDF curves are larger than those estimated from the outputs of GCMs for all future scenarios for the period of 2015–2056. This finding indicates that for the study area, the Cov-IDF curves is capable of capturing the climate change signal for at least future 50 years. Another meaningful comparison is provided by Lee et al. (2020). They established a nonstationary model whose parameters varied with surface air temperature (SAT) and/or dew-point temperature (DPT), and the future projections of these two covariates produced from various GCMs were input to the established nonstationary model to predict future rainfall distributions. The design rainfall depths calculated from the nonstationary model are compared with those obtained directly from the GCMs’ simulations of

future rainfall, and it is found that the future design precipitation indirectly yielded by the nonstationary model exhibits much less variation among different GCMs and the spatial variation of rate of change is also consistent among various GCMs.

One of the essential keys of the Cov-IDF curves method is the selection of covariates. [Yan et al. \(2017, 2019b\)](#) highlighted that there are two requirements for covariates in nonstationary frequency analysis: (i) they are associated with the physical processes of extreme events and can describe the variation characteristics of extreme events, and (ii) they can be reliably predicted for the purpose of further providing reliable prediction of the probability distributions of the future extreme rainfall. [Qian et al. \(2022\)](#) comprehensively analyzed the impacts of urbanization on urban extreme precipitation in terms of factors like urban heat island, urban surface roughness, and urban aerosol loading. For the purpose of finding the best covariate to describe the variation properties of extreme rainfall, [Agilan and Umamahesh \(2017\)](#) constructed the nonstationary GEV model with a number of covariates, namely local temperature, urbanization, global warming, Indian Ocean Dipole (IOD), ENSO, and time. Their results showed that local factors like urbanization were the best covariates for urban short-duration extreme rainfall, whereas global factors, such as ENSO and IOD, were the optimal explanatory covariates for urban long-duration extreme rainfall. [Sarhadi and Soulis \(2017\)](#) derived nonstationary IDF curves for the Great Lakes area by constructing the nonstationary GEV models with time and Southern Oscillation Index (SOI), and they confirmed the impacts of low frequency climate signals, i.e., SOI, on the extreme rainfall. However, most of the existing studies concerning adaptation of IDF curves focus on the establishment of nonstationary models just for the historical period, disregarding the future period during which the drainage infrastructures are designed for service. Actually, under the nonstationary context, the distributions of extreme rainfall vary from year to year, and the infrastructure is supposed to suffer different kinds of risk of failure during observation and operation period, respectively. To obtain the future distributions of extreme precipitation, it is necessary to find covariates that can be reliably predicted. [Lee et al. \(2020\)](#) builds nonstationary models using historical SAT or dew-point temperature DPT as covariates, then future SAT and DPT outputs from different climate models are input into the established nonstationary models to analyze the future distribution changes of extreme precipitation. In addition to temperature, some studies have shown that urbanization factors are closely related to the changes in urban extreme precipitation ([Kishtawal et al., 2009; Miao et al., 2011; Agilan and Umamahesh, 2015; Singh et al., 2016; Gao et al., 2018; Gu et al., 2019; Lu et al., 2019; Wang et al., 2021](#)). Therefore, it is reasonable and worthwhile to update IDF curves using climate factor or urbanization factor as covariates.

Another essential key of the Cov-IDF curves method is the estimation of design precipitation. In the time-varying probability distribution model, the design value and the return period are no longer one-to-one, but change with time. Initially, there are studies calculating the time-varying design precipitation ([Zhang et al., 2015; Gao et al., 2016](#)), which is infeasible for engineering practice. To address the issue of nonstationary design for updating IDF curves, a low-risk method is proposed and widely-used, which uses the 95th percentile of time-varying statistical parameters of the established nonstationary model in the historical period as the effective parameter, and to calculate the effective design values corresponding to various return periods ([Cheng et al., 2014; Agilan and Umamahesh, 2016; Song et al., 2020](#)). However, this kind of low-risk method is conservative and just account for the observations in historical period ([Agilan and Umamahesh, 2016; Yan et al., 2022a](#)) and is likely to result in under-investment (increasing trend in future) or over-investment (decreasing trend in future) of municipal engineering infrastructures. Moreover, either the time-varying design method or the conservative effective design method calculates design precipitation just for the observation period, paying little attention to the future period during which the drainage infrastructures are designed for service. Under a changing environment, the municipal infrastructures suffer different risk of failure during historical and operation periods because of the evolution of the nonstationary models. Therefore, nonstationary design precipitation should fully consider the possible evolution of nonstationary models in future operation period of municipal infrastructures and communicate the risk/reliability they will suffer. In the past decade, several nonstationary hydrological design methods were developed, such as the expected number of exceedances (ENE) and expected waiting time (EWT) introduced into the field of hydrology by [Salas and Obeysekera \(2014\)](#). [Yan et al. \(2020\)](#) discussed the applicability of EWT method in practical hydrological engineering design and pointed out that EWT and ENE methods have limitations in considering the impact of design life of projects when calculating the design values. Several methods considering the design lifespan have also been developed, such as the design life level (DLL) ([Rootzén and Katz, 2013](#)), equivalent reliability (ER) ([Hu et al., 2018](#)). [Yan et al. \(2017\)](#) developed the average design life level (ADLL) method based on the average annual reliability ([Read and Vogel, 2015](#)), which considers that the average annual reliability of the hydrological project in the design lifespan under nonstationary conditions should be the same as that of yearly reliability  $1-1/m$  corresponding to the return period  $m$ . The ER and ADLL methods are recommended by [Yan et al. \(2017\)](#) for practical engineering design. However, to our knowledge, there are no studies which have explored the applicability of the ER or ADLL methods in updating the rainfall IDF curves.

Thus, it is important to explore more possible covariates and candidate distributions to better capture the changing characteristics of extreme precipitation, and update the IDF curves using nonstationary design method. The objectives of this study are therefore: (i) to analyze the temporal variation of urban extreme precipitation with different durations (1-h to 48-h); (ii) to investigate what is the optimal nonstationary distributions and what is the best covariate to characterize the changing properties of extreme precipitation, namely local physical processes (e.g., urbanization) or large-scale circulation processes (e.g., ENSO), and (iii) to estimate the design precipitation values using the average annual reliability-based ADLL method and update the current IDF curves. For the purpose of fulfilling these objectives, we used the hourly precipitation data of 8 meteorological stations in Beijing city. First, this paper analyzed the trend of AMP for different durations (1-h, 2-h, 3-h, 4-h, 5-h, 6-h, 12-h, 18-h, 24-h, 36-h and 48-h). Then, different nonstationary models are constructed for the AMP with significant trends, considering the combination of different alternative distribution (lognormal, Gamma, Logistic, Weibull and generalized extreme value distribution), varying types and covariates (time, urbanization, temperature, ENSO, etc.), while for the AMP without significant trends, the conventional stationary method is used to estimate the design precipitation. It should be mentioned that the future annual probability distributions of extreme precipitation are determined by predicting the covariate in future period. Particularly, the future changes of urbanization are predicted by the Cellular Automaton-

Markov (CA-Markov) model. Finally, the IDF curves in Beijing city are updated by integrating both the stationary and nonstationary design rainfall results.

## 2. Study area and data

The location of the Beijing city and the distribution of the associated meteorological stations are shown in Fig. 1. Beijing is located between the geographical coordinates  $115^{\circ}25' E-120^{\circ}43' E$  and  $39^{\circ}26' N-41^{\circ}03' N$  with a total area of about  $16,455 \text{ km}^2$ . The annual average temperature of Beijing is about  $12.9^{\circ}\text{C}$ , and the annual average precipitation is about 600 mm for plain region. Beijing city is core city in the Beijing-Tianjin-Hebei (BTH) economic zone. With the rapid economic growth in Beijing city, the resident population of Beijing has witnessed an increase of 150% from 8.71 million to 21.84 million. Meanwhile, the urbanization process is accelerated in recent decades. The urban built-up area of Beijing is only 395 in 1990, while in 2020, the urban built-up area of Beijing city has reached  $1469 \text{ km}^2$  based on the data from China City Statistical Yearbook provided by the National Bureau of Statistics of China (<http://www.stats.gov.cn/sj/ndsj/>). The accelerating urbanization has greatly changed the land use and land cover of Beijing city.

Hourly precipitation data of the 8 meteorological stations in Beijing city for the period 1954–2018 are obtained from National Meteorological Science Data Center (<http://data.cms.cn/>). Besides, some local and global physical covariates are used to construct the nonstationary distributions. The annual maximum daily temperature is collected from the National Meteorological Science Data Center. Some studies have reported that ENSO and East Asian Summer Monsoon (EASM) have great influence on the extreme precipitation in Beijing city (Zhang et al., 2015; Yuan et al., 2019; Song et al., 2019; Zhang et al., 2022a). Besides, in recent years, some studies have shown that EASM is affected by ENSO and North Atlantic Oscillation (NAO) (Linderholm et al., 2011; Chen et al., 2013). Therefore, in this study, the large-scale circulation processes, including ENSO, NAO and EASM, are also used as covariates. The monthly average NINO 3.4 Sea Surface Temperature anomalies is used to represent the ENSO process, and the annual NINO 3.4 values are determined by averaging the values from July to December, the period when ENSO evolves and attains its peak (Xiao et al., 2017; Li

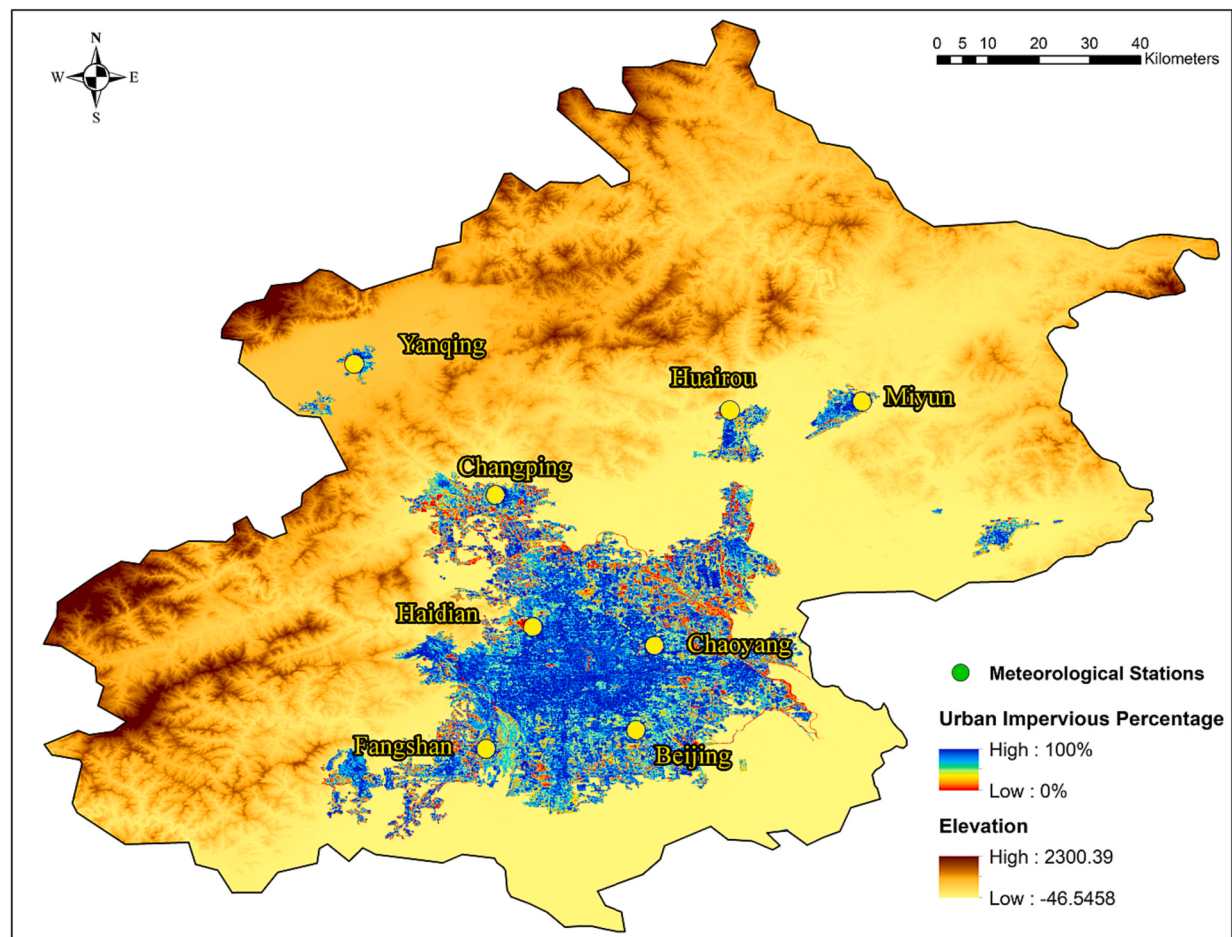


**Fig. 1.** Location map of Beijing city and spatial distribution of the 8 meteorological stations in the study area. The background is the elevation of Beijing city and the blue colour represents high impervious percentage in the core urban area. (For interpretation of the references to colour in this figure legend, the reader is referred to the web version of this article.)

et al., 2021). The above climate index data are accessed from the website of Climate Prediction Center of National Oceanic and Atmospheric Administration (<https://www.cpc.ncep.noaa.gov/data/indices/>). Recent studies have shown that extreme precipitation events are significantly affected by the process of local urbanization (Kishitawal et al., 2009; Miao et al., 2011; Agilan and Umamahesh, 2015; Wu et al., 2019). In this study, the change of urban construction area extracted from the land use and land cover (LULC) in the urban area of Beijing city is employed to reflect the urbanization process. The remote sensing data of LULC for the period 1980–2020 is provided by the Resource Environmental Science and Data Center of Chinese Academy of Sciences (<https://www.resdc.cn/Default.aspx>), and the LULC data of each year is obtained through interpolation. Besides, it should be noted that since we just obtained the LULC data for the period of 1980–2020, the urban construction data for 1954–1979 is estimated based on Lu et al. (2001).

### 3. Methodology

#### 3.1. Trend analysis

In this paper, Mann-Kendall (MK) test is used to analyze the trend of extreme precipitation series. Suppose a stationary independent sequence is  $z_t$  ( $t = 1, 2, \dots, n$ ),  $n$  is the number of observations. The MK test statistic  $S$  is defined as follows

$$S = \sum_{i=1}^{n-1} \sum_{j=i+1}^n Sgn(z_j - z_i) \quad (1)$$

$$Sgn(c) = \begin{cases} +1 & c > 0 \\ 0 & c = 0 \\ -1 & c < 0 \end{cases} \quad (2)$$

When  $n \geq 10$ , the statistic  $S$  is approximately normally distributed whose mean and variance are given by

$$E[S] = 0 \quad (3)$$

$$Var(S) = n(n-1)(2n+5)/18 \quad (4)$$

The standardized test statistic  $U$  is computed by

$$U = \begin{cases} (S - 1) / \sqrt{Var(S)} & S > 0 \\ 0 & S = 0 \\ (S + 1) / \sqrt{Var(S)} & S < 0 \end{cases} \quad (5)$$

The null hypothesis of the MK test is that there exists no significant trend in the examined time series. The significance level of 0.05 and the associated critical value 1.96 are employed in this analysis. So, the detected increasing/decreasing trend is statistically significant only when the value of  $U$  is larger than 1.96.

#### 3.2. Nonstationary precipitation frequency analysis

##### 3.2.1. Construction of the nonstationary models

In this paper, the GAMLS model implemented in R language (Rigby and Stasinopoulos, 2005; Qu et al., 2020) was used to build the nonstationary distributions. For the purpose of exploring possible alternative probability distributions and finding the best covariates for the nonstationary models, we constructed a total of 485 models for each station considering a variety of different combinations of probability distributions, physical covariates and variation types. Three widely employed probability distributions, namely gamma (GA), lognormal (LNO), Weibull (WEI), Logistic (LO) and generalized extreme value (GEV) distributions (Beskow et al., 2015; Gil-leland and Katz, 2016; Li et al., 2019; Yan et al., 2022a; Jiang et al., 2019; Kuang et al., 2018; Yan et al., 2019a), was used. Time, local physical processes (urbanization, annual maximum daily temperature), and global physical processes (ENSO, NAO and EASM) were selected as the covariates to build the nonstationary models.

Under a changing environment, it is assumed that the hydrological series follow the time-varying distributions, whose location parameter  $\mu_t$  and scale parameter  $\sigma_t$  are assumed to vary with selected covariates  $x_b$  using the generalized linear regression function, which is given by

$$h(\mu_t) = \mu_0 + \sum_{b=1}^B \mu_b x_b \quad (6)$$

$$h(\sigma_t) = \sigma_0 + \sum_{b=1}^B \sigma_b x_b \quad (7)$$

where  $h(\cdot)$  represents the link function of statistical parameters,  $x_b$  ( $b = 1, 2, \dots, B$ ) is covariate, and  $B$  is the number of covariates. Besides, the maximum likelihood method is used to estimate the model parameters.

### 3.2.2. Model selection and goodness-of-fit test

In order to avoid model over-fitting, the corrected Akaike Information Criterion (AICc) (Sugahara et al., 2009) is used as an index to select the optimal nonstationary model, and its mathematical expression is given by

$$AICc = GD + 2k + \frac{2k(k+1)}{n-k-1} \quad (8)$$

where  $k$  is the degree of freedom of the model,  $n$  is the sample size,  $GD$  is the global deviation. The lower the AICc value is, the better the fitting quality of the constructed nonstationary distribution.

### 3.2.3. Validation of nonstationary models using split-sample test

Before any projection, it is important to validate the predictive capability of the constructed nonstationary (NS) models and compare it with that of stationary (ST) model. Thus, we used the split-sample test method which leaves some observation data as independent validation sources for our NS model. Specifically in our case, 70% of the observation data is used to calibrate both NS and ST models, and the rest 30% of the observation data is used to validate the predictive capabilities of both NS and ST models based on the likelihood function. Theoretically, the likelihood function offers insights into the credibility of the estimated statistical model in light of the observations from the evaluation period (Yan et al., 2021a; Luke et al., 2017).

$$\begin{cases} L(\theta|z_t^e) = \sum_{t=t_1}^{t_2} g_s(z_t^e|\mu, \sigma) \\ L(\theta_t|z_t^e) = \sum_{t=t_1}^{t_2} g_{ns}(z_t^e|\mu_t, \sigma) \end{cases} \quad (9)$$

where  $g_s(\cdot)$  is the constructed ST model and  $g_{ns}(\cdot)$  is the NS model.  $L(\theta|z_t^e)$  is the likelihood function for observations  $z_t^e$  in the evaluation period  $t_1-t_2$  using ST model, and  $L(\theta_t|z_t^e)$  is the likelihood function for  $z_t^e$  in the evaluation using NS model.

### 3.3. Prediction of land use and cover

In the nonstationary design theory, once we have the optimal nonstationary model constructed in the historical period, we could obtain the future distributions of extreme precipitation by inputting the future prediction of covariates into the established model. In this study, future land use and land cover (LULC) scenarios, representing future urbanization condition of the study area, are predicted by the CA-Markov model (Wang et al., 2020; Pan et al., 2017; Nouri et al., 2014). CA-Markov model combines the Markov chain process and Cellular Automaton (CA) model, and it is a very effective and widely used land use simulation tool. The temporal variations among different land use types are controlled by the Markov chain through the transition matrices, and the variations of spatial pattern are determined by the CA model through the suitability plots. In this study, the CA-Markov model is implemented based on the IDRISI Selva (Eastman, 2009). The land use prediction mainly consists of three steps: (a) the calculation of the LULC transfer matrix from the LULC map using a Markov model; (b) the preparation of suitability plots according to the evaluation indicators in the multiple criteria evaluation module; and (c) the simulation of spatial distribution of urban land use change using the CA model based on the pre-calculated transition matrix and suitability plots.

The Kappa coefficient, which is usually used to assess the consistency between the observed and simulated maps, is used to evaluate the performance of the constructed CA-Markov model, which is described as

$$Kappa = \frac{p_0 - p_c}{1 - p_c} \quad (10)$$

where  $p_0$  is the proportion of the cells which are appropriately simulated;  $p_c$  is the expected proportion correction by chance. If  $Kappa < 0.4$ , the two drawings are greatly different and have low similarity. If  $0.4 \leq Kappa \leq 0.75$ , the difference between the two drawings is obvious and the similarity is general, i.e., there are many grid simulation errors; If  $0.75 < Kappa < 1$ , the difference between the two drawings is small, i.e., the simulation results are better and with high reliability.

### 3.4. Average design life level (ADLL)

The ADLL method is proposed based on the average annual reliability method (Yan et al., 2017; Read and Vogel, 2015). For a future project assumed to be in operation starting from year  $T_1$  to year  $T_2$ , the design lifespan is  $T_2 - T_1 + 1$ . Under the non-stationary context, the average annual reliability  $RE_{T_1-T_2}^{ave}$  over the design lifespan can be expressed as

$$RE_{T_1-T_2}^{ave} = \frac{1}{T_2 - T_1 + 1} \sum_{t=T_1}^{T_2} (1 - p_t) = \frac{1}{T_2 - T_1 + 1} \sum_{t=T_1}^{T_2} G_{z,t}(z_q|\theta_t) \quad (11)$$

where  $G_{z,t}(\cdot)$  is the probability distribution of  $z$ , and  $1 - p_t$  is the non-exceedance probability that an extreme event is smaller than  $z_q$ . ADLL method assumes that, the average annual reliability associated with a nonstationary design quantile should be equal to the

annual reliability  $1 - 1/m$  under the stationary context, i.e.,  $RE_{T_1-T_2}^{\text{ave}} = 1 - 1/m$ , during the design lifespan  $T_1 - T_2$  of a hydrological project. Therefore, the design value  $Z_{T_1-T_2}^{\text{ADLL}}(m)$  of return period  $m$  calculated by the ADLL method can be obtained by

$$\frac{1}{T_2 - T_1 + 1} \sum_{t=T_1}^{T_2} G_{Z,t} \left( Z_{T_1-T_2}^{\text{ADLL}}(m) | \theta_t \right) = 1 - 1/m \quad (12)$$

To comprehensively compare the difference between design rainfall estimated using ST and NS models. In this study, we employed the widely used bootstrap method to calculate the uncertainties of design rainfall for both models. The details of the bootstrap method can be found in [Yan et al. \(2017\)](#).

#### 4. Results and discussion

##### 4.1. Trend analysis

The trends of the extreme rainfall with different durations (1-h, 2-h, 3-h, 4-h, 5-h, 6-h, 12-h, 18-h, 24-h, 36-h and 48-h) of the 8 meteorological stations in the calibration period (1954–1999) were examined using MK test, and the results are shown in [Fig. 2](#). Generally, different levels of trends are observed for various durations at the 8 stations. Among them, for short-duration AMP (smaller than 6-h), most stations show increasing trends or slight decreasing trends, while most stations show decreasing trends for longer durations. Particularly, significant decreasing trend is detected for the 18-h AMP for Beijing station at the significance level of 0.05. Besides, it is found that for Chaoyang, Huairou, Miyun and Yanqing stations, increasing trends are detected for short-durations particularly smaller than 6-h, while for longer durations, decreasing trends are observed. What is interesting is that among the 4 stations, 3 stations (Huairou, Miyun and Yanqing) are located in the northern suburbs of Beijing. That means the trends of short-duration extreme precipitation of Beijing city are different with those of long-durations, which is expected to result in more quick-response and severe urban waterlogging events.

##### 4.2. Nonstationary frequency analysis

In this study, we constructed the nonstationary model for the 18-h AMP of Beijing station based on the MK test. To find the optimal nonstationary model, finally, a total of 485 models were constructed for the calibration period (1954–1999). Among them, the nonstationary lognormal distribution with both location and scale parameters changing with ENSO and EASM is the best model,

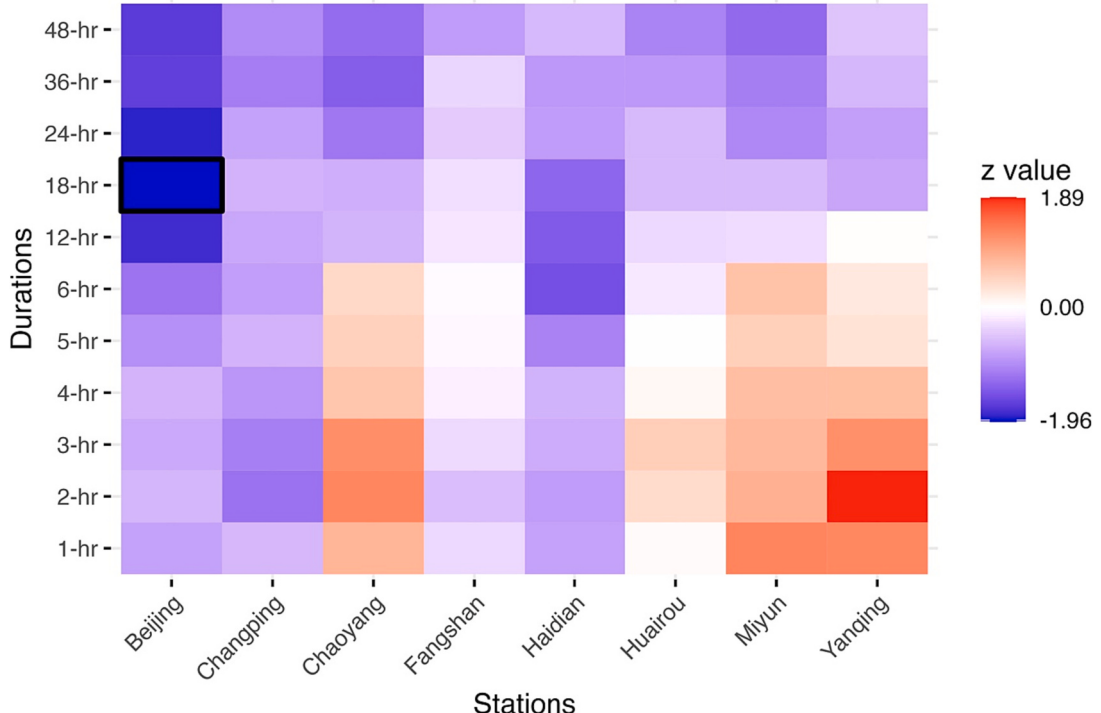


**Fig. 2.** Trend analysis results of AMP for the calibration period (1954–1999) with different durations for 8 stations in Beijing. The duration with significant trend at the 0.05 significance level is marked with black box. The warm colors indicate increasing trends whereas the cold colors represent decreasing trends.

denoted by NS-EE, with the lowest AICc value (461.6). However, the biggest challenge for the best model is the difficulty of projection of future long-term (30 years) values of ENSO and EASM. As highlighted by Yan et al. (2017), the covariates used in the estimation of future design rainfall are supposed to be reliably projected using well-designed method, to reduce the uncertainties of design rainfall. Thus, in this study we employed the nonstationary model with location parameter changing with urbanization, denoted by NS-U, to estimate the design rainfall. The NS-U model has an AICc value of 463.6 and is ranked among the top 5% models out of all the 485 models.

Next, we will validate the performance of both NS-EE and NS-U in comparison to the stationary model (ST) for the observations in the validation period from 2000 to 2018. For NS-EE model, the joint likelihood of obtaining the observations in the validation period is improved by 219%, compared with the ST model, while the joint likelihood of observing results with the NS-U model during the validation period decreased by 81% compared with the ST model. If we check the annual likelihood of obtaining each observation in the validation period, it is found that the overall performance of NS-U and NS-EE is better than that of ST model (Fig. 3). It should be noted that all models fail to get the extreme rainfall in 2016, which is the second largest rainfall in 65 years. Interestingly, if we ignore the extreme rainfall in 2016, the joint likelihood of NS-U would be improved by 316% compared with that of ST. Besides, it is seen that the trend of AMP (increasing) in the validation period is different than that in calibration period (decreasing) (Fig. 3), which means the constructed trend in the calibration period will reverse, and this situation is expected to be unfavorable for the NS models. Even though, the performance of both NS-EE and NS-U is satisfactory in the validation period.

#### 4.3. Prediction of future land use change

In this section, we will predict the future changes of LULC using the CA-Markov model as a reflection of urbanization process in the study area, since we have selected NS-U model as the optimal model for estimation of design rainfall. In this study, to evaluate the performance of the CA-Markov model, based on the observation data of LULC in 2010 (LULC2010) and in 2015 (LULC2015), the LULC in 2020 (LULC2020) was projected using a CA-Markov model, and was compared with the observation data of LULC2020. To be specific, first, a Markov model was utilized to determine the transition matrix between LULC2010 and LULC2015. And then, indicators such as slope, distance from the traffic line, and distance from the center of the city were selected to draw a map of the suitability of LULC change (Fig. 4). Finally, the LULC2020 was simulated based on observation data of LULC2015, estimated transition matrix and suitability maps using the CA-Markov model (Fig. 5). The kappa coefficient between the observed and simulated LULC2020 is 0.79,

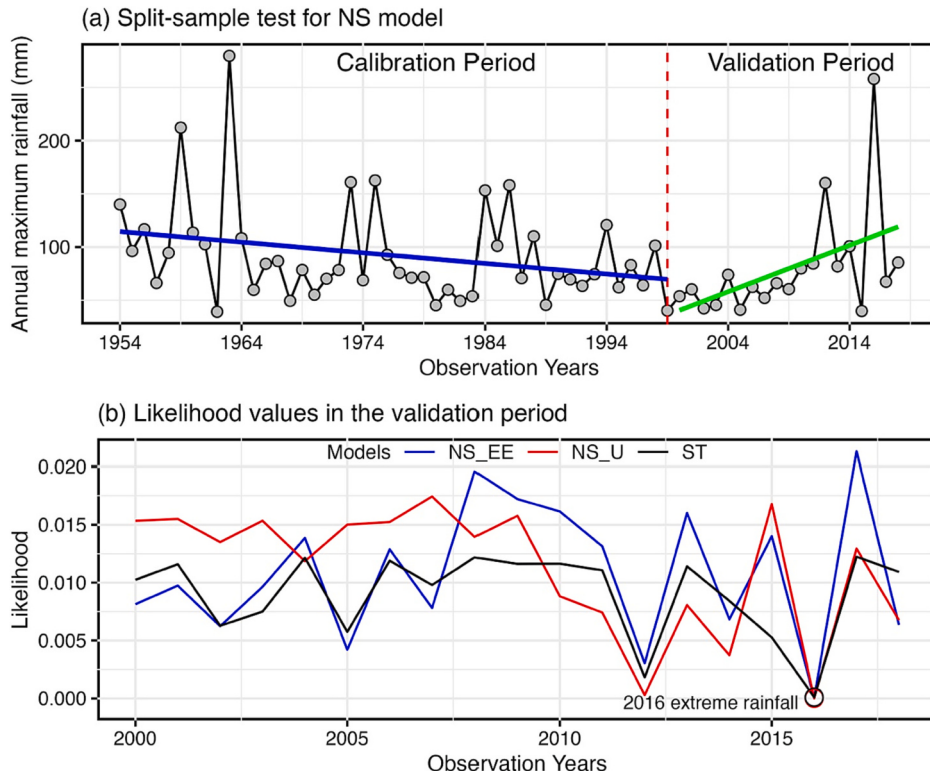


**Fig. 3.** The calibration period (1954–1999) and validation period (2000–2018) of the Beijing station and their associated trends (a); Likelihood values of the observations using NS and ST models in the validation period (2000–2018) (b). NS\_EE denotes the NS model changing with ENSO and EASM, while NS\_U denotes the NS model changing with urbanization covariate. It should be mentioned that the extreme rainfall in 2016 is the second-largest extreme rainfall in 65 years.

indicating that the simulated LULC2020 has a high agreement with the observed LCLU2020, and the strong ability of CA-Markov model to simulate LCLU.

After the verification of the predictive capability of the CA-Markov model, it is used to determine the transition matrix between LUC2015 and LUC2020, and then simulates the LULC of the study area for the next 30 years based on the observed LULC2020 data, the transfer matrix, and the suitability maps. As shown in Fig. 5, there is an increase in the city building land area, and the level of urbanization is in an increasing state. The fast-growing urbanization process, which leads to the urban heat island, is expected to have an impact on extreme precipitation in the study area. Finally, the area of urban construction land is extracted to represent the urbanization process, and input into the established nonstationary model to predict the future change of distributions of extreme precipitation.

#### 4.4. Estimation of design precipitation

##### 4.4.1. Comparison of design precipitation under stationary and nonstationary contexts

Assume a municipal project is designed to be in service for 2020–2050, we can predict the future distributions of extreme precipitation for each year based on the constructed nonstationary model (NS-U) and the simulated urbanization covariate for 2020–2050. It should be mentioned that in the split-sample test, we showed the results of trend analysis using MK just for the calibration period (Fig. 2). Here, when we estimated the ST and NS design rainfall, we performed the MK test for the whole observation period, again, and it was found that AMP with durations 12-h, 18-h, 24-h, and 48-h showed significant trends at the 0.05 significance level (supplement material Figs. S1 and S2). Although the trend of AMP with 36-h duration is not significant ( $p$ -value = 0.06), NS design method was also implemented from a practical engineering perspective, making it more comprehensible and relevant for the public and decision-makers. Then, the design precipitation for the durations of 12-h, 18-h, 24-h, 36-h and 48-h during the design life 2020–2050 is estimated using the average annual reliability-based ADLL method, and the corresponding uncertainties are also estimated using the bootstrap method. As shown in Fig. 6, take the AMP of 18-h in Beijing station as an example, the design rainfall calculated by stationary method is larger than that calculated using nonstationary design method, indicating that the stationary design method overestimates the design rainfall, which is supposed to increase the project cost. In addition, the differences between the stationary design rainfall and nonstationary design rainfall increase slightly from 18.2% to 20.2% with the increase of return periods. What is interesting is that the difference of uncertainties associated with nonstationary and stationary design values decrease with the increase of return periods ( $T$ ), which are 34% ( $T = 10$ ), 16.5% ( $T = 50$ ) and 12.6% ( $T = 100$ ). The ADLL method is able to consider the design lifespan of municipal projects and is a reliable method to estimate the design precipitation under nonstationary contexts.

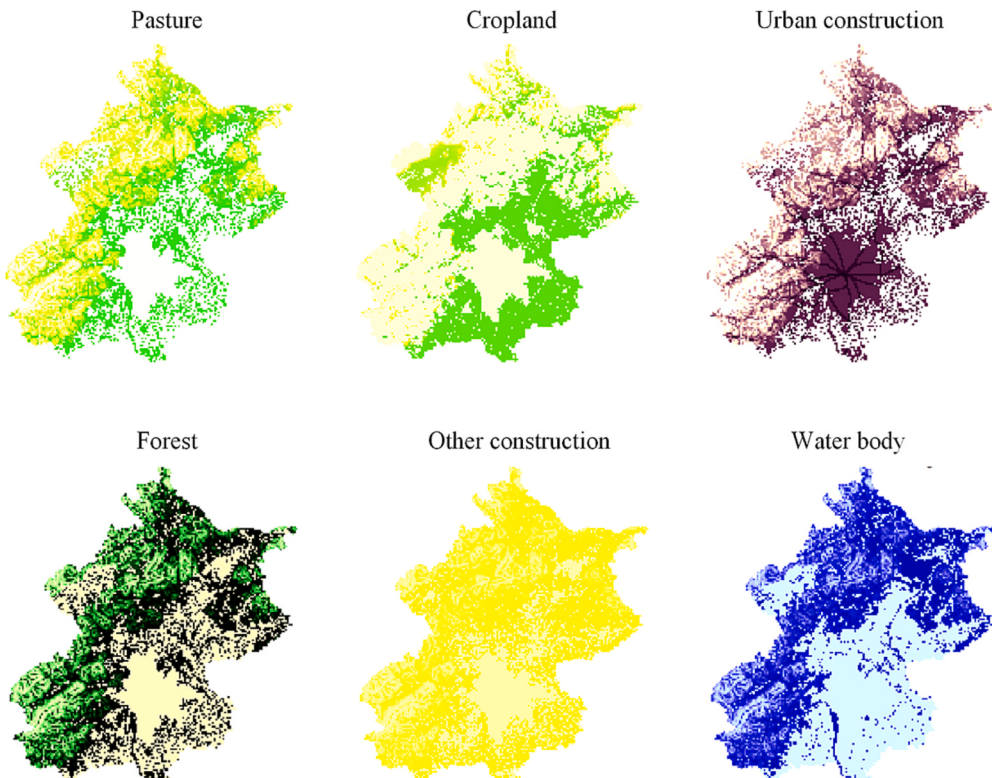


**Fig. 4.** Suitability plots of different land use types in 2015–2020. The higher the values in each land use type, the better is the suitability.

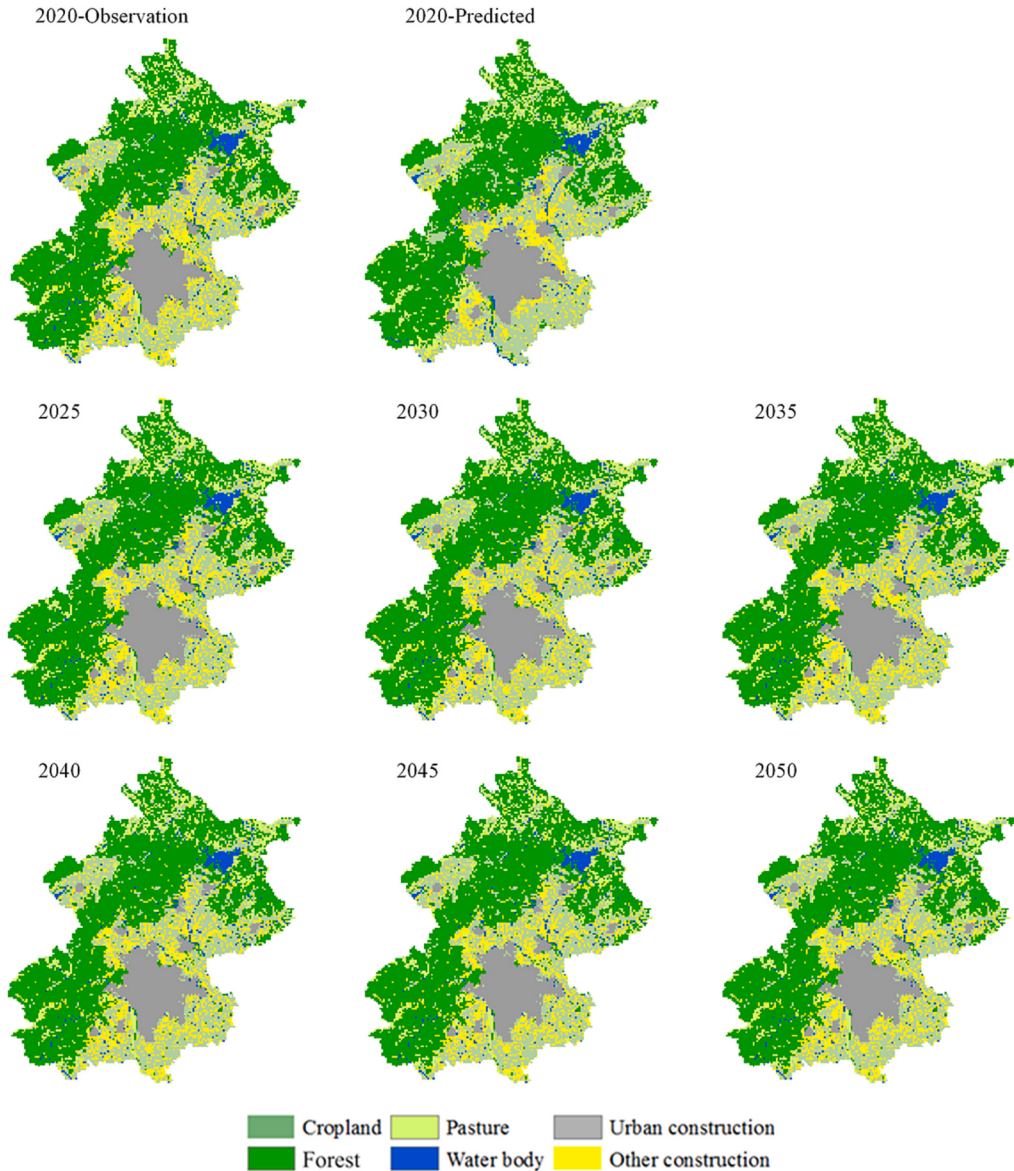


**Fig. 5.** Prediction of future LULC change (2025–2050) in Beijing city based on CA-Markov model. The observed and predicted LULC maps of 2020 are present to check the performance of the CA-Markov model.

#### 4.4.2. Derivation of IDF curves

In this section, we will update the IDF curves for Beijing station which shows significant trend in this study. It should be mentioned that for durations without significant trends, the ST model and design strategy are still used to calculate the design rainfall, and the future stationary IDF is the same as the historical IDF under the stationary context. Based on the trend analysis, for each duration of extreme precipitation with significant trend (12-h, 18-h, 24-h, 36-h and 48-h), the nonstationary model is constructed and the ADLL design method is used to estimate design precipitation. While for the durations of extreme precipitation without significant trends (1-h, 2-h, 3-h, 4-h, 5-h, and 6-h), the conventional stationary model is still constructed, and the stationary design method is used to estimate the design precipitation. Finally, by integrating the design results of both stationary and nonstationary methods, the updated IDF curves corresponding to 2-year, 10-year, 50-year and 100-year return periods under a changing environment are derived and compared with the IDF curves created under stationary conditions. In addition, the uncertainties associated with IDF are provided to make a comprehensive comparison between NS and ST IDF curves.

As can be seen in Fig. 7, for extreme precipitation showing a decreasing trend, the stationary IDF curves overestimate their precipitation intensities in comparison with the updated IDF curve. In addition, as the duration of rainfall increases, the gap between IDF curves under ST and NS conditions becomes less pronounced across all return periods. For instance, the difference in design rainfall between NS and ST conditions for a 50-year return period stands at 2.8 mm/h for a 12-h duration. However, this gap narrows to 0.9

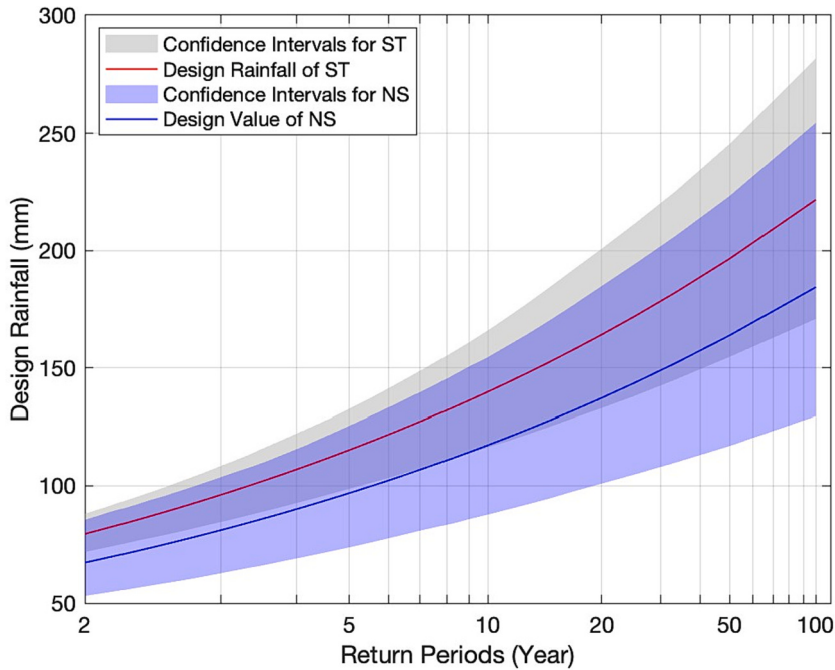


**Fig. 6.** The design rainfall and associated uncertainties using NS and ST methods for 18-h duration extreme rainfall in Beijing station for future period of 2020–2050. The blue and red solid lines are NS and ST design rainfall, respectively, and the light blue and light grey ribbons are the uncertainties associated with NS and ST design rainfall, respectively. (For interpretation of the references to colour in this figure legend, the reader is referred to the web version of this article.)

mm/h when the duration extends to 48 h. Furthermore, this difference becomes larger with the increase of return period. At the 18-h duration, the difference in design rainfall between NS and ST is 0.7 mm/h for a 2-year return period, but this jumps to 2.1 mm/h for a 100-year return period. Concerning design uncertainties, as expected, both the NS and ST design uncertainties generally become larger with longer return periods, which is anticipated given that we estimate 100-year design values using just 65 years of observations. What's intriguing, however, is that the disparity between NS and ST design uncertainties becomes less pronounced as the return periods increase. For instance, the difference for an 18-h, 2-year design rainfall is 0.83 mm/h, but for an 18-h, 100-year design rainfall, this difference narrows to 0.21 mm/h. From another point of view, the uncertainties diminish as the duration of rainfall lengthens. To illustrate, when analyzing the uncertainties between NS and ST for a 10-year design rainfall, there's a noticeable gap of 1.4 mm/h at a 12-h duration. However, this gap shrinks to just 0.32 mm/h when the duration extends to 48 h. Thus, for Beijing station in this study, if we still use the stationary IDF curves in practical municipal engineering applications, it will increase the investment of urban infrastructures in certain degree, particularly when withstanding extreme precipitation with shorter duration (e.g., 12-h) and longer return periods. Moreover, the uncertainty between NS and ST design methods becomes narrow with longer durations and return periods, which will facilitate the application of NS design strategy in practical municipal engineering design. Therefore, based on the above results, it is necessary to update IDF curve under a changing environment.

#### 4.5. Discussion

In recent decades, a lot of evidence concerning the increase of urban extreme short-duration precipitation have been provided in meteorological and hydrological communities (Yan et al., 2021b; Westra et al., 2014). In a changing world, design strategies to update the IDF curves are critical for design of urban drainage infrastructures to resist potential increase of risk of failure (Yan et al., 2021b; Ganguli and Coulibaly, 2017). In addition, some national governments have highlighted the need to update the IDF design guidelines. For example, it is strengthened by the guidelines of Canadian water practitioner that we should update the IDF curves more frequently than before time to better consider the possible changes of characteristics of urban extreme precipitation in Canada (CSA (Canadian Standards Association), 2010). However, there is no consensus about what method should be used to update the IDF curves. In this study, we tried to update the IDF curves using the nonstationary method. But it should be mentioned that there are still several aspects to be improved in future study for updating of the IDF curves.

Firstly, we should be more cautious about the selection of covariate. In this study, we investigated the possibility of several different kinds of covariate and selected the best covariate for each duration of extreme precipitation. We demonstrate the superiority of the physical covariates, particular the large-scale climate variability and local urbanization, in comparison with time covariate. But for Beijing station, the best covariates, namely ENSO and EASM, could not be reliably predicted in future long-period, and we selected the urbanization covariate (top 5% best model) to estimate the design values. In future, we should explore more physical processes,

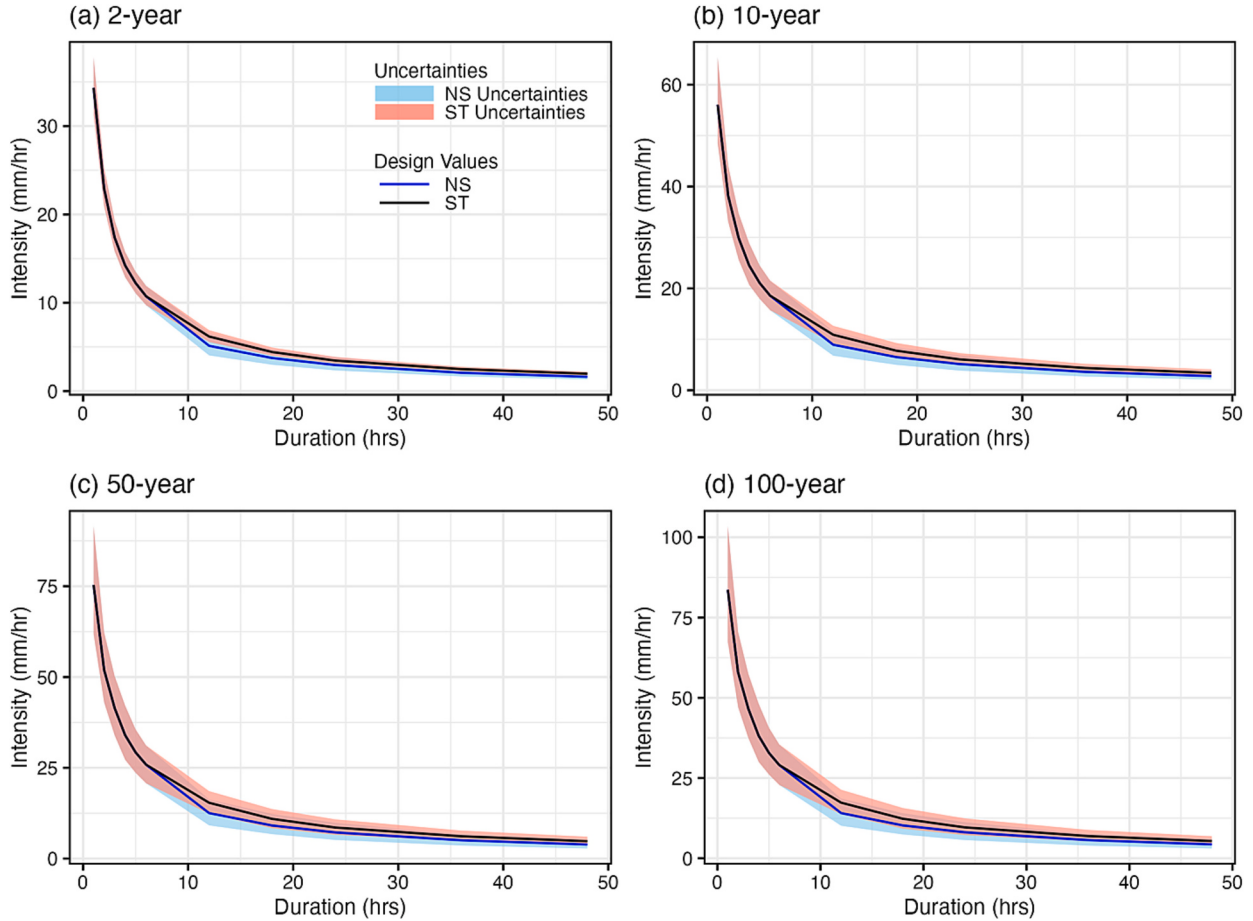


**Fig. 7.** The updated IDF curves of Beijing station for the future period of 2020–2050 for various durations and different return periods, namely 2-year (a), 10-year (b), 50-year (c) and 100-year (d). The blue and black solid lines are NS and ST design rainfall, respectively, and the light blue and light red ribbons are the uncertainties associated with NS and ST design rainfall, respectively. (For interpretation of the references to colour in this figure legend, the reader is referred to the web version of this article.)

associated with extreme precipitation, to drive the NS model, and meanwhile improve the predictive capability of the covariates. Indeed, there consists of uncertainties in parameter estimation and covariate prediction. Thus, how to evaluate these uncertainties associated with the nonstationary design strategy is very important for updating IDF curves.

Secondly, both the Cov-IDF and the Clim-IDF have their own advantages and disadvantages. Cov-IDF is based on the sub-daily observations and enables us to investigate the impacts of external physical covariates on the statistical characteristics of precipitation, but it depends on the assumption that the estimated relationship between covariates and parameters is the same as in future period, which maybe unreal. On the contrary, Clim-IDF is based on the physically based climate models, and it is easier to estimate the design rainfall using the stationary design strategy, but the temporal and spatial resolution is not enough for constructing the IDF curves. So, extra spatiotemporal downscaling is needed (Hosseinzadehtalaei et al., 2020; Zhang et al., 2022b). In addition, the uncertainties of Cov-IDF result from the model structure, projection of future covariates, and the design method, whereas the uncertainties of Clim-IDF mainly result from the uncertainties of climate models and the spatiotemporal downscaling method. It should be mentioned that Zhang et al. (2022a) tried to improve the accuracy of Clim-IDF curves using an ensemble forecasting method based on the vine copula theory. Thus, efforts should be made to combine these two methods. For instance, Lee et al. (2020) used both the nonstationary model and the GCMs' projections to update the IDF curves. They developed a nonstationary model and used the air temperature or dew-point temperature to describe the variation of its statistical parameters. The future simulations of two selected covariates from GCMs were input to the pre-established nonstationary model to predict the distributions of future extreme precipitation. Another well-designed attempt is demonstrated by Rago et al. (2018). They employed the outputs of multiple GCMs as the future forecast of extreme precipitation, and then they derived the updated IDF curves using the nonstationary extreme value analysis. In future study, researchers should take the advantages of both the two methods and provide more reliable adaptation of the IDF curves.

Thirdly, as mounting evidence shows the relationship between urbanization and extreme precipitation, it would be interesting to examine the spatial heterogeneity of urbanization in the nonstationary IDF curves. It is expected to find different trends for urban core

area and urban fringe and corresponding the importance of urbanization on the nonstationary IDF curves is expected to be different. An interesting investigation can be found in [Zhang et al. \(2022b\)](#). They compared the relative changes in past and future sub-daily (3-h) and 24-h extreme precipitation over BTH and found that there are minimal changes in the intensity of extreme rainfall for 3-h and 24-h duration for the core area of BTH. However, the outskirts of the city have seen an increase of at least 40%. In this study, although we have collected 8 stations in Beijing city, only the Beijing station exhibits significant trend and nonstationary models are developed just for Beijing station. We are not able to check the importance of urbanization on nonstationary IDF curves. In future studies, we could collect more extreme rainfall data for the whole BTH region and analyze the spatial heterogeneity of urbanization on IDF curves.

Finally, we are living in a changing environment, and the urban municipal projects are expected to suffer different levels of risks during their design life due to the ongoing changes in the characteristics of extreme precipitation. Therefore, the updated future IDF curves should account for the design lifespan of municipal projects to communicate potential future climate risks during its design life. In future studies, apart from the average annual reliability based ADLL design method, more nonstationary design methods accounting for the design lifespan of the municipal projects should be developed.

## 5. Conclusion

In this study, we examined the trend of extreme precipitation with various durations for 8 stations in Beijing city. Then, we constructed a range of nonstationary models for the extreme precipitation with significant trends to explore what is the optimal nonstationary distribution and what is the best covariate to explain the changes of extreme precipitation. We employed different probability distributions (GEV, LNO and GA) and different kinds of covariates, namely time, local physical processes (temperature and urbanization), and global physical processes (ENSO, NAO and EASM) to describe the different variation types of the statistical parameters. For the purpose of predicting future distributions of extreme precipitation, future changes of urbanization (urban construction area) were predicted using the CA-Markov model. After that, the nonstationary design precipitation was estimated using the average annual reliability based ADLL method, while the stationary method was used to estimate design precipitation for other durations of extreme precipitation without significant trends. Finally, the IDF curves of the study area were updated by incorporating the design results of the stationary and nonstationary methods. The main conclusions are summarized as follows:

- (1) For urban short-duration extreme rainfall (shorter than 6-h) in Beijing, most stations display either increasing trends or minor decreasing trends. In contrast, decreasing trends are detected for long-duration extreme rainfall (longer than 12-h) across all stations.
- (2) The predictive accuracy of the optimal NS model, changing with ENSO and EASM, surpasses that of the ST model by 219% during the validation period, highlighting the significant benefits of integrating physical covariates.
- (3) The stationary IDF curves are supposed to underestimate the design precipitation for extreme precipitation with durations longer than 12-h, compared with the updated IDF curves. In addition, the difference between NS and ST design uncertainties becomes narrower for longer duration design rainfall.
- (4) the updated IDF curves, calculated using the average annual reliability based ADLL method, are able to account for the design lifespan of the municipal engineering, and it will reduce the risk of failure of urban infrastructures or avoid unnecessary project cost.

## Code availability

The code used in this study are available from the corresponding author on reasonable request.

## CRediT authorship contribution statement

**Lei Yan:** Conceptualization, Methodology, Funding acquisition, Writing – review & editing, Supervision. **Dongyang Lu:** Writing – original draft, Data curation, Visualization. **Lihua Xiong:** Funding acquisition, Writing – review & editing. **Hongfeng Wang:** Data curation, Resources. **Qinghua Luan:** Funding acquisition, Resources. **Cong Jiang:** Formal analysis, Validation. **Bin Xiong:** Formal analysis. **Wentao Xu:** Data curation. **Pengtao Yan:** Software, Visualization. **Qingwen Lei:** Software. **Chong-Yu Xu:** Supervision, Writing – review & editing.

## Declaration of Competing Interest

The authors declare that they have no known competing financial interests or personal relationships that could have appeared to influence the work reported in this paper.

## Data availability

The data used in this study are available from the corresponding author on reasonable request.

## Acknowledgement

This study is financially supported jointly by the National Natural Science Foundation of China (No. 51909053, U2240201, 52109002), the Research Council of Norway (FRINATEK Project 274310, KLIMAFORSK Project 302457), the Youth Foundation of Education Department of Hebei Province (QN2019132), the Key Research and Development Project of Hebei Province (20375401D), Natural Science Foundation of Jiangxi Province (20212BAB214066), Xingtai City Science and Technology Bureau (2021ZZ032), Science and Technology Project of Hebei Education Department (BJ2019023), all of which are greatly appreciated.

## Appendix A. Supplementary data

Supplementary data to this article can be found online at <https://doi.org/10.1016/j.uclim.2023.101701>.

## References

- Agilan, V., Umamahesh, N.V., 2015. Detection and attribution of non-stationarity in intensity and frequency of daily and 4-h extreme rainfall of Hyderabad, India. *J. Hydrol.* 530, 677–697. <https://doi.org/10.1016/j.jhydrol.2015.10.028>.
- Agilan, V., Umamahesh, N.V., 2016. Is the covariate based non-stationary rainfall IDF curve capable of encompassing future rainfall changes? *J. Hydrol.* 541, 1441–1455. <https://doi.org/10.1016/j.jhydrol.2016.08.052>.
- Agilan, V., Umamahesh, N.V., 2017. What are the best covariates for developing non-stationary rainfall intensity-duration-frequency relationship? *Adv. Water Resour.* 101, 11–22. <https://doi.org/10.1016/j.advwatres.2016.12.016>.
- Alam, M.S., Elshorbagy, A., 2015. Quantification of the climate change-induced variations in intensity-duration-frequency curves in the Canadian prairies. *J. Hydrol.* 527, 990–1005. <https://doi.org/10.1016/j.jhydrol.2015.05.059>.
- Allen, M.R., Ingram, W.J., 2002. Constraints on future changes in climate and the hydrologic cycle. *Nature* 419 (6903). <https://doi.org/10.1038/nature01092>.
- Beskow, S., Caldeira, T.L., de Mello, C.R., Faria, L.C., Guedes, H.A.S., 2015. Multiparameter probability distributions for heavy rainfall modeling in extreme southern Brazil. *J. Hydrol. Reg. Stud.* 4, 123–133. <https://doi.org/10.1016/j.ejrh.2015.06.007>.
- Bekaz, N., Šraj, M., Mikoš, M., 2016. Copula-based IDF curves and empirical rainfall thresholds for flash floods and rainfall-induced landslides. *J. Hydrol.* 541, 272–284. <https://doi.org/10.1016/j.jhydrol.2016.02.058>.
- Chen, W., Feng, J., Wu, R., 2013. Roles of ENSO and PDO in the link of the East Asian winter monsoon to the following summer monsoon. *J. Clim.* 26 (2), 622–635. <https://doi.org/10.1175/JCLI-D-12-00021.1>.
- Cheng, L., Aghakouchak, A., 2014. Nonstationary precipitation intensity-duration-frequency curves for infrastructure design in a changing climate. *Sci. Rep.* 4 (1), 378–381. <https://doi.org/10.1038/srep07093>.
- Cheng, L., Aghakouchak, A., Gillette, E., Katz, R.W., 2014. Non-stationary extreme value analysis in a changing climate. *Clim. Chang.* 127, 353–369. <https://doi.org/10.1007/s10584-014-1254-5>.
- CSA (Canadian Standards Association), 2010. Technical Guide-Development, Interpretation and Use of Rainfall Intensity-Duration-Frequency (IDF) Information: Guideline for Canadian Water Resources Practitioners. CSA Group, Ottawa.
- Eastman, J.R., 2009. IDRISI Guide to GIS and Image Processing Accessed in IDRISI Selva, 17. Clark University, Worcester, MA, p. 182e185.
- Endreyn, T.A., Imbeah, N., 2009. Generating robust rainfall intensity-duration-frequency estimates with short-record satellite data. *J. Hydrol.* 371, 182–191. <https://doi.org/10.1016/j.jhydrol.2009.03.027>.
- Evans, J.P., Westra, S., 2012. Investigating the mechanisms of diurnal rainfall variability using a regional climate model. *J. Clim.* 25 (20), 7232–7247. <https://doi.org/10.1175/JCLI-D-11-00616.1>.
- Farnham, D.J., Doss-Gollin, J., Lall, U., 2018. Regional extreme precipitation events: robust inference from credibly simulated GCM variables. *Water Resour. Res.* 54 (6), 3809–3824. <https://doi.org/10.1002/2017WR021318>.
- Feng, Z., Leung, L.R., Hagos, S., Houze, R.A., Burleyson, C.D., Balaguru, K., 2016. More frequent intense and long-lived storms dominate the springtime trend in central US rainfall. *Nat. Commun.* 7, 13429. <https://doi.org/10.1038/ncomms13429>.
- Fowler, H.J., Ekström, M., Blenkinsop, S., Smith, A.P., 2007. Estimating change in extreme European precipitation using a multimodel ensemble. *J. Geophys. Res. Atmos.* 112 (D18) <https://doi.org/10.1029/2007JD008619>.
- Fowler, H.J., Lenderink, G., Prein, A.F., Westra, S., Allan, R.P., Ban, N., Barbero, R., Berg, P., Blenkinsop, S., Do, H.X., Guerreiro, S., Haerter, J.O., Kendon, E.J., Lewis, E., Schaer, C., Sharma, A., Villarini, G., Wasko, C., Zhang, X., 2021. Anthropogenic intensification of short-duration rainfall extremes. *Nat. Rev. Earth Environ.* 2, 107–122. <https://doi.org/10.1038/s43017-020-00128-6>.
- Ganguli, P., Coulibaly, P., 2017. Does nonstationarity in rainfall require nonstationary intensity-duration-frequency curves? *Hydrolog. Earth Syst. Sci.* 21 (12), 6461–6483. <https://doi.org/10.5194/hess-21-6461-2017>.
- Gao, M., Mo, D., Wu, X., 2016. Nonstationary modeling of extreme precipitation in China. *Atmos. Res.* 182, 1–9. <https://doi.org/10.1016/j.atmosres.2016.07.014>.
- Gao, L., Huang, J., Chen, X., Chen, Y., Liu, M., 2018. Contributions of natural climate changes and human activities to the trend of extreme precipitation. *Atmos. Res.* 205, 60–69. <https://doi.org/10.1016/j.atmosres.2018.02.006>.
- Gilleland, E., Katz, R.W., 2016. extRemes 2.0: an extreme value analysis package in R. *J. Stat. Softw.* 72 (8), 1–39. <https://doi.org/10.18637/jss.v072.i08>.
- Gu, X., Zhang, Q., Li, J., Singh, V.P., Sun, P., 2019. Impact of urbanization on nonstationarity of annual and seasonal precipitation extremes in China. *J. Hydrol.* 575, 638–655. <https://doi.org/10.1016/j.jhydrol.2019.05.070>.
- Gu, X., Ye, L., Xin, Q., Zhang, C., Zeng, F., Nerantzaki, S.D., Papalexiou, S.M., 2022. Extreme precipitation in China: a review. *Adv. Water Resour.* 163, 104144. <https://doi.org/10.1016/j.advwatres.2022.104144>.
- Guerreiro, S.B., Fowler, H.J., Barbero, R., Westra, S., Lenderink, G., Blenkinsop, S., Lewis, E., Li, X., 2018. Detection of continental-scale intensification of hourly rainfall extremes. *Nat. Clim. Chang.* 8, 803–807. <https://doi.org/10.1038/s41558-018-0245-3>.
- Hansen, J., Ruedy, R., Sato, M., Lo, K., 2010. Global surface temperature change. *Rev. Geophys.* 48 (4), RG4004 <https://doi.org/10.1029/2010RG000345>.
- Hassanzadeh, E., Nazemi, A., Adamowski, J., Nguyen, T., Van-Nguyen, V., 2019. Quantile-based downscaling of rainfall extremes: Notes on methodological functionality, associated uncertainty and application in practice. *Adv. Water Resour.* 131, 103371. <https://doi.org/10.1016/j.advwatres.2019.07.001>.
- Hosseiniزاده‌الائی, P., Tabari, H., Willems, P., 2020. Climate change impact on short-duration extreme precipitation and intensity-duration-frequency curves over Europe. *J. Hydrol.* 590, 125249. <https://doi.org/10.1016/j.jhydrol.2020.125249>.
- Hu, Y., Liang, Z., Singh, V.P., Zhang, X., Wang, J., Li, B., Wang, H., 2018. Concept of equivalent reliability for estimating the design flood under non-stationary conditions. *Water Resour. Manag.* 32 (2), 997–1011. <https://doi.org/10.1007/s11269-017-1851-y>.
- IPCC, 2021. In: *Climate Change 2021: The Physical Science Basis. Contribution of Working Group I to the Sixth Assessment Report of the Intergovernmental Panel on Climate Change*. Cambridge University Press (In Press).
- Jiang, C., Xiong, L., Yan, L., Dong, J., Xu, C.-Y., 2019. Multivariate hydrologic design methods under nonstationary conditions and application to engineering practice. *Hydrolog. Earth Syst. Sci.* 23 (3), 1683–1704. <https://doi.org/10.5194/hess-23-1683-2019>.

- Kishtawal, C.M., Niyogi, D., Tewari, M., Pielke, R.A., Shepherd, J.M., 2009. Urbanization signature in the observed heavy rainfall climatology over India. *Int. J. Climatol.* 30 (13), 1908–1916. <https://doi.org/10.1002/joc.2044>.
- Kourtis, I.M., Tsibintzis, V.A., 2021. Adaptation of urban drainage networks to climate change: a review. *Sci. Total Environ.* 771, 145431. <https://doi.org/10.1016/j.scitotenv.2021.145431>.
- Kourtis, I.M., Tsibintzis, V.A., 2022. Update of intensity-duration-frequency (IDF) curves under climate change: a review. *Water Supply*. <https://doi.org/10.2166/ws.2022.152> ws2022152.
- Kuang, Y., Xiong, L., Yu, K., Liu, P., Xu, C.-Y., Yan, L., 2018. Comparison of first-order and second-order derived moment approaches in estimating annual runoff distribution. *J. Hydrol. Eng.* 23 (8), 04018034 [https://doi.org/10.1061/\(ASCE\)HE.1943-5584.0001683](https://doi.org/10.1061/(ASCE)HE.1943-5584.0001683).
- Lee, O., Sim, I., Kim, S., 2020. Application of the non-stationary peak-over threshold methods for deriving rainfall extremes from temperature projections. *J. Hydrol.* 585, 124318. <https://doi.org/10.1016/j.jhydrol.2019.124318>.
- Lenderink, G., Fowler, H.J., 2017. Hydroclimate: understanding rainfall extremes. *Nat. Clim. Chang.* 7 (6), 391–393. <https://doi.org/10.1038/nclimate3305>.
- Lenderink, G., Van Meijgaard, E., 2008. Increase in hourly precipitation extremes beyond expectations from temperature changes. *Nat. Geosci.* 1 (8), 511–514. <https://doi.org/10.1038/ngeo262>.
- Li, L., Yao, N., Li Liu, D., Song, S., Lin, H., Chen, X., Li, Y., 2019. Historical and future projected frequency of extreme precipitation indicators using the optimized cumulative distribution functions in China. *J. Hydrol.* 579, 124170. <https://doi.org/10.1016/j.jhydrol.2019.124170>.
- Li, X., Zhang, K., Gu, P., Feng, H., Yin, Y., Chen, W., Cheng, B., 2021. Changes in precipitation extremes in the Yangtze River basin during 1960–2019 and the association with global warming, ENSO, and local effects. *Sci. Total Environ.* 760, 144244. <https://doi.org/10.1016/j.scitotenv.2020.144244>.
- Lima, C.H.R., Kwon, H.-H., Kim, Y.-T., 2018. A local-regional scaling-invariant Bayesian GEV model for estimating rainfall IDF curves in a future climate. *J. Hydrol.* <https://doi.org/10.1016/j.jhydrol.2018.08.075>.
- Linderholm, H.W., Ou, T.H., Jeong, J.H., Folland, C.K., Gong, D., Liu, H., Liu, Y., Chen, D., 2011. Interannual teleconnections between the summer North Atlantic oscillation and the East Asian summer monsoon. *J. Geophys. Res.-Atmos.* 116, D13107 <https://doi.org/10.1029/2010JD015235>.
- Lu, Q., Zhan, J., Ren, G., 2001. A primary study on urbanization, land use/cover change and the related social-human factors in Beijing in the past 100 years. *Geogr. Res.* 20 (6), 688–696 (in Chinese with English abstract).
- Lu, M., Xu, Y., Shan, N., Wang, Q., Yuan, J., Wang, J., 2019. Effect of urbanisation on extreme precipitation based on nonstationary models in the Yangtze River Delta metropolitan region. *Sci. Total Environ.* 673, 64–73. <https://doi.org/10.1016/j.scitotenv.2019.03.413>.
- Lu, F., Song, X., Xiao, W., Zhu, K., Xie, Z., 2020. Detecting the impact of climate and reservoirs on extreme floods using nonstationary frequency models. *Stoch. Env. Res. Risk A* 34, 169–182. <https://doi.org/10.1007/s00477-019-01747-2>.
- Lucas-Picher, P., Argüeso, D., Brisson, E., Tramblay, Y., Berg, P., Lemonsu, A., Kotlarski, S., Caillaud, C., 2021. Convection-permitting modeling with regional climate models: latest developments and next steps. *Wiley Interdiscip. Rev. Clim. Chang.* 12 (6), e731 <https://doi.org/10.1002/wcc.731>.
- Luke, A., Vrugt, J.A., Aghakouchak, A., Matthew, R., Sanders, B.F., 2017. Predicting nonstationary flood frequencies: evidence supports an updated stationarity thesis in the United States. *Water Resour. Res.* 53 (7), 5469–5494. <https://doi.org/10.1002/2016WR019676>.
- Martel, J.L., Brissette, F.P., Lucas-Picher, P., Troin, M., Arsenault, R., 2021. Climate change and rainfall intensity-duration-frequency curves: overview of science and guidelines for adaptation. *J. Hydrol. Eng.* 26 (10), 03121001 [https://doi.org/10.1061/\(ASCE\)HE.1943-5584.0002122](https://doi.org/10.1061/(ASCE)HE.1943-5584.0002122).
- Meinshausen, M., Meinshausen, N., Hare, W., Raper, S.C.B., Frieler, K., Knutti, R., Allen, M.R., 2009. Greenhouse-gas emission targets for limiting global warming to 2°C. *Nature* 458, 1158–1162. <https://doi.org/10.1038/nature08017>.
- Miao, S., Chen, F., Fan, Q., 2011. Impacts of urban processes and urbanization on summer precipitation: a case study of heavy rainfall in Beijing on 1 August 2006. *J. Appl. Meteorol. Climatol.* 50 (4), 806–825. <https://doi.org/10.1175/2010JAMC2513.1>.
- Mondal, A., Mujumdar, P.P., 2015. Modeling non-stationarity in intensity, duration and frequency of extreme rainfall over India. *J. Hydrol.* 521, 217–231. <https://doi.org/10.1016/j.jhydrol.2014.11.071>.
- Nouri, J., Gharagozlou, A., Arjmandi, R., Faryadi, S., Adl, M., 2014. Predicting urban land use changes using a CA-Markova model. *Arab. J. Sci. Eng.* 39, 5565–5573. <https://doi.org/10.1007/s13369-014-1119-2>.
- Ouarda, T.B., Yousef, L.A., Charron, C., 2019. Non-stationary intensity-duration-frequency curves integrating information concerning teleconnections and climate change. *Int. J. Climatol.* 39 (4), 2306–2323. <https://doi.org/10.1002/joc.5953>.
- Pan, S., Liu, D., Wang, Z., Zhao, Q., Zou, H., Hou, Y., Liu, P., Xiong, L., 2017. Runoff responses to climate and land use/cover changes under future scenarios. *Water* 9 (7), 475. <https://doi.org/10.3390/w9070475>.
- Qian, Y., Chakraborty, T.C., Li, J., Li, D., He, C., Sarangi, C., Chen, F., Yang, X., Leung, L.R., 2022. Urbanization impact on regional climate and extreme weather: current understanding, uncertainties, and future research directions. *Adv. Atmos. Sci.* 39 (6), 819–860. <https://doi.org/10.1007/s00376-021-1371-9>.
- Qu, C., Li, J., Yan, L., Yan, P., Cheng, F., Lu, D., 2020. Non-stationary flood frequency analysis using cubic B-spline-based GAMLSS model. *Water* 12 (7), 1867. <https://doi.org/10.3390/w12071867>.
- Ragno, E., Aghakouchak, A., Love, C.A., Cheng, L., Vahedifard, F., Lima, C.H.R., 2018. Quantifying changes in future intensity-duration-frequency curves using multimodel ensemble simulations. *Water Resour. Res.* 54 (3), 1751–1764. <https://doi.org/10.1002/2017WR021975>.
- Read, L.K., Vogel, R.M., 2015. Reliability, return periods, and risk under nonstationarity. *Water Resour. Res.* 51 (8), 6381–6398. <https://doi.org/10.1002/2015WR017089>.
- Rigby, R.A., Stasinopoulos, D.M., 2005. Generalized additive models for location, scale and shape. *J. Roy. Stat. Soc. C-Appl. Stat.* 54 (3), 507–554. <https://doi.org/10.1111/j.1467-9876.2005.00510.x>.
- Rootzen, H., Katz, R.W., 2013. Design life level: quantifying risk in a changing climate. *Water Resour. Res.* 49 (9), 5964–5972. <https://doi.org/10.1002/wrcr.20425>.
- Salas, J.D., Obeysekera, J., 2014. Revisiting the concepts of return period and risk for nonstationary hydrologic extreme events. *J. Hydrol. Eng.* 19 (3), 554–568. [https://doi.org/10.1061/\(ASCE\)HE.1943-5584.0000820](https://doi.org/10.1061/(ASCE)HE.1943-5584.0000820).
- Sarhadi, A., Soulis, E.D., 2017. Time-varying extreme rainfall intensity-duration-frequency curves in a changing climate. *Geophys. Res. Lett.* 44 (5), 2454–2463. <https://doi.org/10.1002/2016GL072201>.
- Schleff, K.E., Kunkel, K.E., Brown, C., Demissie, Y., Lettenmaier, D.P., Wagner, A., Wigmosta, M.S., Karl, T.R., Easterling, D.R., Wang, K.J., François, B., Yan, E., 2023. Incorporating non-stationarity from climate change into rainfall frequency and Intensity-Duration-Frequency (IDF) curves. *J. Hydrol.* 616, 128757. <https://doi.org/10.1016/j.jhydrol.2022.128757>.
- Silva, D.F., Simonovic, S.P., Schardon, A., Goldenfum, J.A., 2021. Assessment of non-stationary IDF curves under a changing climate: case study of different climatic zones in Canada. *J. Hydrol. Reg. Stud.* 36, 100870 <https://doi.org/10.1016/j.ejrh.2021.100870>.
- Singh, J., Vittal, H., Karmakar, S., Ghosh, S., Niyogi, D., 2016. Urbanization causes nonstationarity in Indian summer monsoon rainfall extremes. *Geophys. Res. Lett.* 43 (21), 11,269–11,277. <https://doi.org/10.1002/2016gl071238>.
- Song, X., Zou, X., Zhang, C., Zhang, J., Kong, F., 2019. Multiscale spatiotemporal changes of precipitation extremes in Beijing-Tianjin-Hebei region, China during 1958–2017. *Atmosphere* 10 (8), 462. <https://doi.org/10.3390/atmos10080462>.
- Song, X., Zou, X., Mo, Y., Zhang, J., Zhang, C., Tian, Y., 2020. Nonstationary bayesian modeling of precipitation extremes in the Beijing-Tianjin-Hebei region, China. *Atmos. Res.* 242, 105006. <https://doi.org/10.1016/j.atmosres.2020.105006>.
- Su, C., Chen, X., 2019. Covariates for nonstationary modeling of extreme precipitation in the Pearl River Basin, China. *Atmos. Res.* 229, 224–239. <https://doi.org/10.1016/j.atmosres.2019.06.017>.
- Sugahara, S., Rocha, R.P., Silveira, R., 2009. Non-stationary frequency analysis of extreme daily rainfall in São Paulo, Brazil. *Int. J. Climatol.* 29 (9), 1339–1349. <https://doi.org/10.1002/joc.1760>.
- Vinnarasi, R., Dhanya, C.T., 2022. Time-varying intensity-duration-frequency relationship through climate-informed covariates. *J. Hydrol.* 604, 127178. <https://doi.org/10.1016/j.jhydrol.2021.127178>.
- Vu, T.M., Mishra, A.K., 2019. Nonstationary frequency analysis of the recent extreme precipitation events in the United States. *J. Hydrol.* 575, 999–1010. <https://doi.org/10.1016/j.jhydrol.2019.05.090>.

- Wang, J., Xu, Y., Wang, Y., Yuan, J., Wang, Q., Xiang, J., 2019. Non-stationarity analysis of extreme water level in response to climate change and urbanization in the Taihu Basin, China. *Stoch. Env. Res. Risk A.* 33, 891–904. <https://doi.org/10.1007/s00477-019-01666-2>.
- Wang, Q., Xu, Y., Wang, Y., Zhang, Y., Xiang, J., Xu, Y., Wang, J., 2020. Individual and combined impacts of future land-use and climate conditions on extreme hydrological events in a representative basin of the Yangtze River Delta, China. *Atmos. Res.* 236 (C) <https://doi.org/10.1016/j.atmosres.2019.104805>.
- Wang, J., Cheng, F., Doan, Q.-V., Xu, Y., 2021. Exploring the effect of urbanization on hourly extreme rainfall over Yangtze River Delta of China. *Urban Clim.* 36, 100781. <https://doi.org/10.1016/j.uclim.2021.100781>.
- Westra, S., Fowler, H.J., Evans, J.P., Alexander, L.V., Berg, P., Johnson, F., Kendon, E.J., Lenderink, G., Roberts, N.M., 2014. Future changes to the intensity and frequency of short-duration extreme rainfall. *Rev. Geophys.* 52, 522–555. <https://doi.org/10.1002/2014RG000464>.
- Willems, P., 2013. Revision of urban drainage design rules after assessment of climate change impacts on precipitation extremes at Uccle, Belgium. *J. Hydrol.* 496, 166–177. <https://doi.org/10.1016/j.jhydrol.2013.05.037>.
- Wu, M., Luo, Y., Chen, F., Wong, W.K., 2019. Observed link of extreme hourly precipitation changes to urbanization over coastal South China. *J. Appl. Meteorol. Climatol.* 58 (8), 1799–1819. <https://doi.org/10.1175/JAMC-D-18-0284.1>.
- Xiao, M., Zhang, Q., Singh, V.P., 2017. Spatiotemporal variations of extreme precipitation regimes during 1961–2010 and possible teleconnections with climate indices across China. *Int. J. Climatol.* 37 (1), 468–479. <https://doi.org/10.1002/joc.4719>.
- Xiong, L., Yan, L., Du, T., Yan, P., Li, L., Xu, W., 2019. Impacts of climate change on urban extreme rainfall and drainage infrastructure performance: a case study in Wuhan City, China. *Irrig. Drain.* 68 (2), 152–164. <https://doi.org/10.1002/ird.2316>.
- Xu, Q., Chen, J., Peart, M.R., Ng, C.N., Hau, B.C., Law, W.W., 2018. Exploration of severities of rainfall and runoff extremes in ungauged catchments: a case study of Lai Chi Wo in Hong Kong, China. *Sci. Total Environ.* 634, 640–649.
- Xu, W., Xiong, L., Yan, L., Dong, L., Jiang, C., Xu, C.-Y., 2023. Estimating the scale parameter of the norming constants method in analysing nonstationary annual maximum floods. *Hydrolog. Process.* 37 (2), e14797 <https://doi.org/10.1002/hyp.14797>.
- Yan, L., Xiong, L., Guo, S., Xu, C.-Y., Xia, J., Du, T., 2017. Comparison of four nonstationary hydrologic design methods for changing environment. *J. Hydrol.* 551, 132–150. <https://doi.org/10.1016/j.jhydrol.2017.06.001>.
- Yan, L., Xiong, L., Ruan, G., Xu, C.-Y., Yan, P., Liu, P., 2019a. Reducing uncertainty of design floods of two-component mixture distributions by utilizing flood timescale to classify flood types in seasonally snow covered region. *J. Hydrol.* 574, 588–608. <https://doi.org/10.1016/j.jhydrol.2019.04.056>.
- Yan, L., Li, L., Yan, P., He, H., Li, Jing, Lu, D., 2019b. Nonstationary flood hazard analysis in response to climate change and population growth. *Water* 11 (9), 1811. <https://doi.org/10.3390/w11091811>.
- Yan, L., Xiong, L., Luan, Q., Jiang, C., Yu, K., Xu, C.-Y., 2020. On the applicability of the expected waiting time method in nonstationary flood design. *Water Resour. Manag.* 34, 2585–2601. <https://doi.org/10.1007/s11269-020-02606-4>.
- Yan, L., Xiong, L., Jiang, C., Zhang, M., Wang, D., Xu, C.-Y., 2021a. Updating intensity–duration–frequency curves for urban infrastructure design under a changing environment. *Wiley Interdiscip. Rev. Water* 8 (3), e1519. <https://doi.org/10.1002/wat2.1519>.
- Yan, L., Xiong, L., Ruan, G., Zhang, M., Xu, C.-Y., 2021b. Design flood estimation with varying record lengths in Norway under stationarity and nonstationarity scenarios. *Hydrolog. Res.* 52 (6), 1596–1614. <https://doi.org/10.2166/nh.2021.026.F>.
- Yan, L., Lu, D., Hu, P., Yan, P., Xu, Y., Qi, J., Liu, F., Li, J., 2022a. Estimation of design precipitation in Beijing-Tianjin-Hebei region under a changing climate. *Hydrolog. Sci. J.* 67 (11), 1722–1739. <https://doi.org/10.1080/02626667.2022.2080554>.
- Yan, L., Lei, Q., Jiang, C., Yan, P., Ren, Z., Liu, B., Liu, Z., 2022b. Climate-informed monthly runoff prediction model using machine learning and feature importance analysis. *Front. Environ. Sci.* 10, 1049840. <https://doi.org/10.3389/fenvs.2022.1049840>.
- Yuan, J., Emura, K., Farnham, C., Alam, M.A., 2018. Frequency analysis of annual maximum hourly precipitation and determination of best fit probability distribution for regions in Japan. *Urban Clim.* 24, 276–286. <https://doi.org/10.1016/j.uclim.2017.07.008>.
- Yuan, J., Xu, Y., Wu, L., Wang, J., Wang, Y., Xu, Y., Dai, X., 2019. Variability of precipitation extremes over the Yangtze River Delta, eastern China, during 1960–2016. *Theor. Appl. Climatol.* 138, 305–319. <https://doi.org/10.1007/s00704-019-02829-5>.
- Yue, Z., Xiong, L., Zha, X., Liu, C., Chen, J., Liu, D., 2022. Impact of thresholds on nonstationary frequency analyses of peak over threshold extreme rainfall series in Pearl River Basin, China. *Atmos. Res.* 106269 <https://doi.org/10.1016/j.atmosres.2022.106269>.
- Zhang, D., Yan, D., Wang, Y., Lu, F., Liu, S., 2015. GAMLSS-based nonstationary modeling of extreme precipitation in Beijing-Tianjin-Hebei region of China. *Nat. Hazards* 77 (2), 1037–1053. <https://doi.org/10.1007/s11069-015-1638-5>.
- Zhang, W., Villarini, G., Wehner, M., 2019. Contrasting the responses of extreme precipitation to changes in surface air and dew point temperatures. *Clim. Chang.* 154 (1–2), 257–271. <https://doi.org/10.1007/s10584-019-02415-8>.
- Zhang, M., Rojo-Hernández, J.D., Yan, L., Mesa, O.J., Lall, U., 2022a. Hidden tropical pacific sea surface temperature states reveal global predictability for monthly precipitation for sub-season to annual scales. *Geophys. Res. Lett.* 49 (20), e2022GL099572 <https://doi.org/10.1029/2022GL099572>.
- Zhang, B., Wang, S., Moradkhani, H., Slater, L., Liu, J., 2022b. A vine copula-based ensemble projection of precipitation intensity-duration-frequency curves at sub-daily to multi-day time scales. *Water Resour. Res.* 58 (11), e2022WR032658 <https://doi.org/10.1029/2022WR032658>.
- Zhu, Q., Gu, H., Zhang, X., Xu, Y., 2016. Parameter uncertainty and non-stationarity in regional rainfall frequency analysis in Qu River Basin, East China. *J. Hydrol. Eng.* 21 (5), 0401600 [https://doi.org/10.1061/\(ASCE\)HE.1943-5584.0001355](https://doi.org/10.1061/(ASCE)HE.1943-5584.0001355).
- Zittis, G., Bruggeman, A., Camera, C., Hadjinicolaou, P., Lelieveld, J., 2017. The added value of convection permitting simulations of extreme precipitation events over the eastern Mediterranean. *Atmos. Res.* 191, 20–33. <https://doi.org/10.1016/j.atmosres.2017.03.002>.